Available online at www.sciencedirect.com

ScienceDirect

CeramicsInternational

CERAMICS INTERNATIONAL

www.elsevier.com/locate/ceramint

Effect of barium content on dielectric and energy storage properties of (Pb,La,Ba)(Zr,Sn,Ti)O_3 ceramics

Qian Zhang[a,b], Xiaolin Liu[a], Yong Zhang[b,*], Xiaozhen Song[b], Jia Zhu[b], Ivan Baturin[c], Jianfeng Chen[a]

[a]*State Key Laboratory of Organic-Inorganic Composites, Beijing University of Chemical Technology, Beijing 100029, China*

[b]*Beijing Key Laboratory of Fine Ceramics, State Key Laboratory of New Ceramics and Fine Processing, Institute of Nuclear and New Energy Technology, Tsinghua University, Beijing 100084 China*

[c]*Ferroelectric Laboratory, Institute of Natural Science, Ural Federal University, Ekaterinburg 620000, Russia*

Abstract

The effect of barium content on phase development, dielectric property and energy storage performance of $(Pb_{0.925-x}La_{0.05}Ba_x)(Zr_{0.52}Sn_{0.39}Ti_{0.09})O_3$ (PLBZST) ceramics synthesized by a solid state reaction method was investigated. X-ray diffraction patterns and scanning electron microscopy micrographs illustrated that the pyrochlore phase was effectively suppressed by the introduction of barium in the $(Pb_{0.925}La_{0.05})(Zr_{0.52}Sn_{0.39}Ti_{0.09})O_3$ (PLZST) ceramics. The increase in maximum dielectric constant and the decrease in both transition temperature and switching field with increasing barium content were due to the decrease in the stability of antiferroelectric phase. The energy storage performance of the barium doped PLZST ceramics was studied by measurements of polarization hysteresis loops and discharge curves. The increase of barium content led to the increase of the energy storage density at first and then slight decrease. The study of cyclic charge–discharge showed that barium doped PLZST ceramic capacitor can withstand up to 10,000 cycles with about 8% energy density loss.

Keywords: C. Dielectric properties; C. Fatigue; E. Capacitors; Barium doped PLZST ceramics

1. Introduction

Lead lanthanum zirconate stannate titanate (PLZST) antiferroelectric (AFE) ceramic materials have been studied extensively over the past several decades for applications in high energy storage capacitors [1,2] and high strain actuators/transducers [3,4]. The chemical modifications of PLZST ceramics with La and Sr as well as rare-earth elements were found to be effective in tailoring their dielectric properties. A particularly interesting chemical modifier is barium. It was found that incorporating barium to the A-site of the ABO_3 perovskite structure increased the dielectric constant and decreased the Curie temperature. In addition, barium addition to the PLZST ceramics reduces the switching field and narrows hysteresis loops [5,6]. These changes are attributed to the fact that barium is a ferroelectric (FE) phase stabilizer [7]. In addition, barium doping could improve the fatigue property [8], suppress the stress sensitivity of the phase transition [9], and stabilize the perovskite structure in pyrochlore-prone compositions [10].

Recently, there is an increasing number of researchers using hysteresis loops to obtain the energy storage density, but such measurement cannot estimate real discharge energy density and discharge speed. A resistance, inductance, and capacitance (*RLC*) load circuit was employed to investigate the discharge energy density and discharge speed of antiferroelectric ceramic capacitors [11,12]. It was also utilized for the lifetime estimation of polymer ceramic nanocomposite capacitors and multilayer ceramic capacitors for submicrosecond discharge applications [13]. Besides, a resistance load circuit is one of the promising alternatives to measure the discharge speed and discharged energy density. Xu et al. applied this method to

*Corresponding author. Tel.: +86 10 80194055; fax: +86 10 89796022.
E-mail address: yzhang@tsinghua.edu.cn (Y. Zhang).

investigate the discharge speed and backward phase switching time of PLZST thin films [14]. Recently, it was demonstrated that the discharge time is controlled mainly by the capacitance (C) of samples and the external resistor (R), while the released energy density did not change greatly with various RC values [15,16]. However, there are few reports on the measurements of discharge curves and released energy density of barium doped PLZST ceramics with the resistance load circuit.

In the present study, the energy storage performance was investigated in $(Pb_{0.925-x}La_{0.05}Ba_x)(Zr_{0.52}Sn_{0.39}Ti_{0.09})O_3$ (PLBZST, x=0, 0.02, 0.04, 0.06, 0.08, and 0.10) ceramics synthesized by the solid state reaction method. The charge/discharge energy storage density of the barium doped PLZST ceramics was studied by the hysteresis loops and direct discharge curves measurements. The microstructure and the dielectric properties of the studied ceramics were analyzed to explain the energy storage performance. The fatigue performance of the barium doped PLZST ceramics during cyclic charge–discharge was also studied.

2. Material and methods

The PLBZST powders were prepared by the solid state reaction method. The amount of reagent grade raw materials such as Pb_3O_4, La_2O_3, $BaCO_3$, ZrO_2, $SrCO_3$, TiO_2, and SnO_2 (Sinopharm chemical reagent Co., Ltd., Beijing, China) was weighed according to the formula $(Pb_{0.925-x}La_{0.05}Ba_x)(Zr_{0.52}Sn_{0.39}Ti_{0.09})O_3$ (x=0, 0.02, 0.04, 0.06, 0.08, and 0.10). To prevent lead loss during high temperature, an excess of 1.5 wt% Pb_3O_4 was added. The mixture was milled in polyethylene jars with zirconia balls for 6 h in deionized water. After drying, the mixture was calcined at 1070 °C for 2 h to synthesize PLBZST powders. $Pb(Mg_{0.5}W_{0.5})O_3$ was added into the PLBZST powders to promote sinterability of the bodies and fabricate high density PLBZST ceramics at low temperature. $Pb(Mg_{0.5}W_{0.5})O_3$ was synthesized by a two-stage process starting from the raw materials of Pb_3O_4, WO_3, $(MgCO_3)_4 \cdot Mg(OH)_2 \cdot 5H_2O$ (Sinopharm chemical reagent Co. Ltd., Beijing, China). The wolframite precursor $MgWO_4$ was prepared by calcining a stoichiometric mixture of $(MgCO_3)_4 \cdot Mg(OH)_2 \cdot 5H_2O$ and WO_3 at 1000 °C for 2 h. Then stoichiometric amount of Pb_3O_4 was mixed with $MgWO_4$, and the mixture was calcined at 800 °C for 2 h to obtain $Pb(Mg_{0.5}W_{0.5})O_3$ powders. Then the PLBZST powders were mixed with 5 wt% PMW and 0.05 wt% MnO_2 by re-milling. After drying, the powders were mixed with a small amount of polyvinyl acetate (PVA) binder and uniaxially pressed under a pressure of 4 MPa to form disk-shaped pellets with 10 mm in diameter and 0.6 mm in thickness. After binder burnout, the pressed disks were sintered at 1150 °C with 2 h soaking period in a closed crucible.

The morphology of the fracture surfaces of samples was observed by a scanning electron microscope (SEM, FEI Quanta 200 FEG). An X-ray diffractometer (XRD, Model-D8 Advance, Bruker AXS, Karlsruhe, Germany) was used to determine the phase evolution of the synthesized PLBZST powders. To measure the dielectric properties, silver paste was coated to form electrodes on both sides of the samples and subsequently fired at 600 °C for 20 min. The temperature dependence of the dielectric constant and loss was measured at 1 kHz by means of an LCR meter (HP 4284) interfaced with a computer, during heating at a constant rate of 5 °C/min. The polarization–electric field (P–E) hysteresis loops were measured at room temperature by a classical Sawyer-Tower capacitive voltage divider in a computerized measuring system. All electric fields were supplied by a high voltage power supply (Trek 609-B, NY, USA) driven by an arbitrary waveform generator (HP 33220A, CA, USA). The amplitude of the applied electric field was from 1 to 10 kV/mm.

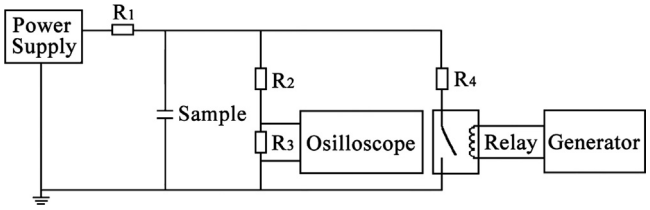

Fig. 1. Circuit diagram of the setup for discharge curve measurement.

The discharge curves were measured with a resistance load circuit as shown in Fig. 1. The sample was firstly charged by a high voltage power supply (Trek 609-B, NY, USA) through the large resistance R_1 in order to keep the charge current within the limit of the supply and minimize the influence on the discharge current. Then the sample was discharged through resistance R_4 using a high voltage relay controlled by the waveform generator. The voltage across the resistance R_3 was recorded with an oscilloscope (TDS 1002B, Tektronix, Beaverton, OR, USA) and the voltage across the sample was calculated by voltage divider based on the resistances R_2 and R_3. Then discharge current was calculated based on the calculated sample voltage and discharge resistor R_4. Discharge time was controlled by selecting the load resistor R_4 and the capacitance of the sample. In this case, the capacitance of the PLBZST samples was from 600 to 1200 pF and the external load resistance R_4=3 MΩ was chosen to keep the discharge time in the order of milliseconds. The influence of the power supply on discharge current was minimized using resistance R_1 much higher than R_4. On the other hand, the value of the resistance of R_2+R_3 was selected to be much higher than R_1 and R_4 to minimize its influence on the voltage across the sample.

3. Results and discussion

The SEM images in Fig. 2 show the fractured surfaces of $(Pb_{0.925-x}La_{0.05}Ba_x)(Zr_{0.52}Sn_{0.39}Ti_{0.09})O_3$ ceramics, where x=0, 0.02, 0.04, 0.06, 0.08, and 0.10. The microstructure of all samples looks quite dense and the grain size of different compositions is barely affected by barium addition. At the composition $x < 0.08$, the smaller grains of the second phase were observed. At $x \geq 0.08$, most of the grains were of regular and equiaxed morphology, typical of perovskite structure ceramics. It indicates that the barium addition has influence on the morphology of the PLBZST ceramics.

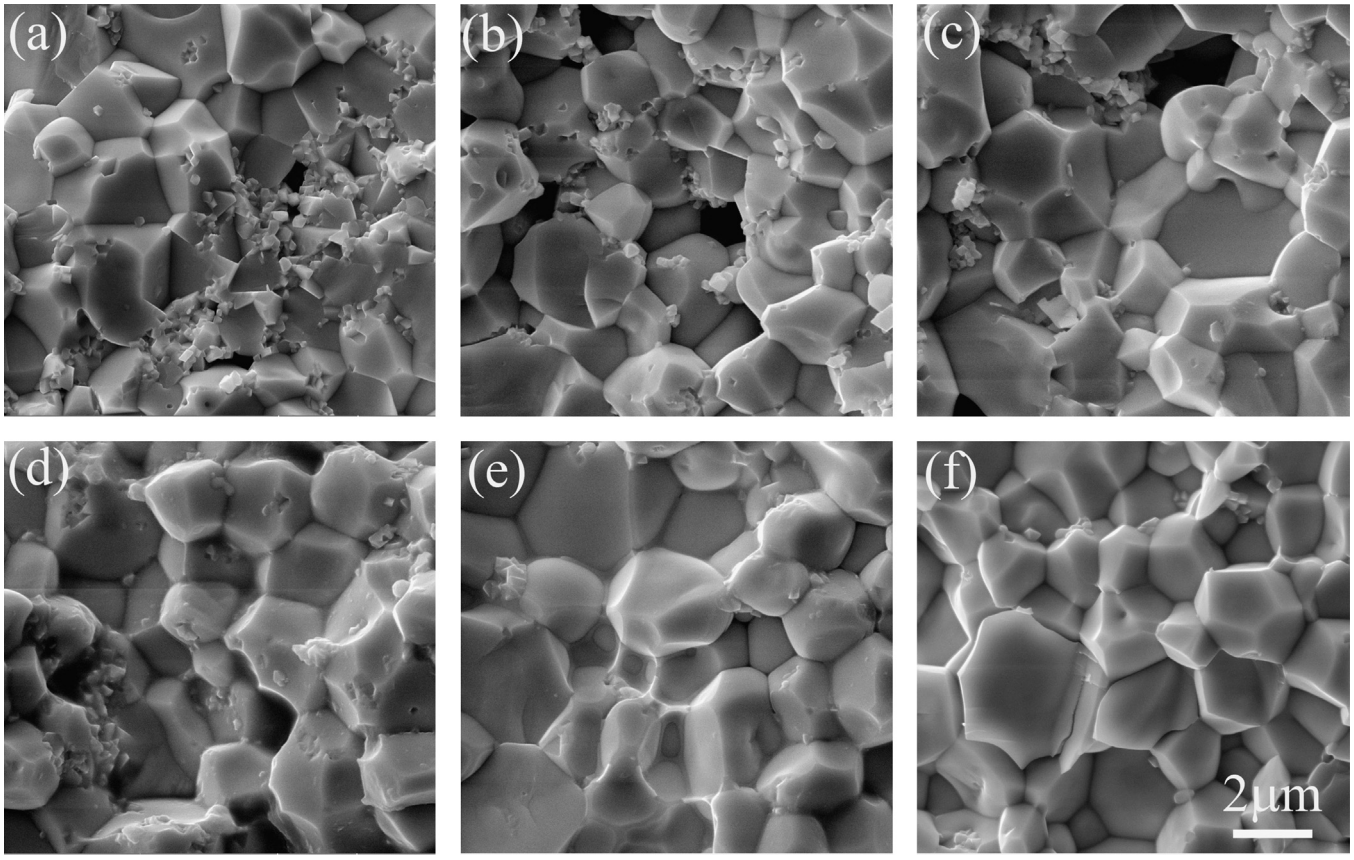

Fig. 2. SEM microstructures of the barium doped PLZST ceramics: (a) 0 mol%, (b) 2 mol%, (c) 4 mol%, (d) 6 mol%, (e) 8 mol% and (f) 10 mol%.

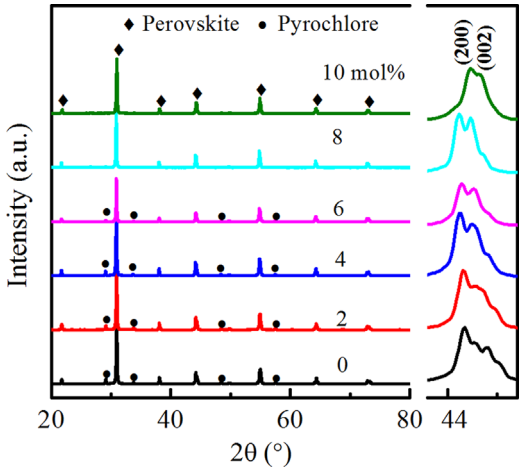

Fig. 3. X-ray diffraction patterns of the PLZST ceramics with different barium contents. The enlarged region for the diffraction peaks at $2\theta=45^{\circ}$.

The XRD patterns of the PLBZST ceramics with various barium contents (Fig. 3) confirm the formation of the perovskite phase with small peaks corresponding to the pyrochlore phase formed during the synthesis. With the increase of barium content, the diffraction peaks of the pyrochlore structure were gradually weakened and disappeared above $x=0.08$, which indicates the increase of the perovskite phase percentage in the studied ceramics. Phase stability of the perovskite structure can be evaluated in terms of tolerance factor τ, which is defined as follows:

$$\tau = \frac{R_A + R_O}{\sqrt{2}(R_B + R_O)} \tag{1}$$

where R_A, R_B, and R_O are the ionic radii of A-site cation, B-site cation, and oxygen anion, respectively. The ionic radii of A-site cation and B-site cation of PLBZST ceramics were expressed by

$$R_A = (0.925 - x)R_{Pb^{2+}} + 0.05R_{La^{3+}} + xR_{Ba^{2+}} \tag{2}$$

$$R_B = 0.52R_{Zr^{4+}} + 0.39R_{Sn^{4+}} + 0.09R_{Ti^{4+}} \tag{3}$$

In general, when the value of τ is close to 1, the perovskite phase will be formed [17]. A tolerance factor lower than 0.9 or higher than 1.1 typically makes the perovskite structure unstable due to a mismatch between preferred A–O and B–O bond lengths [18]. For $\tau < 1$, samples with higher tolerance factor will favor the formation of the perovskite structure. The ionic radii for Pb^{2+}, La^{3+}, Ba^{2+}, Zr^{4+}, Sn^{4+}, Ti^{4+} and O^{2-} are 0.149, 0.136, 0.161, 0.072, 0.069, 0.0605 and 0.135 nm, respectively [19]. According to these formulae, the calculated tolerance factors τ were 0.965, 0.966, 0.967, 0.968, 0.969 and 0.970 for the samples with the barium content of 0, 2, 4, 6, 8 and 10 mol%, respectively. Therefore, barium doping in the PLBZST ceramics exhibits strong effects in promoting the perovskite phase and suppressing the pyrochlore phase in the resulting ceramics.

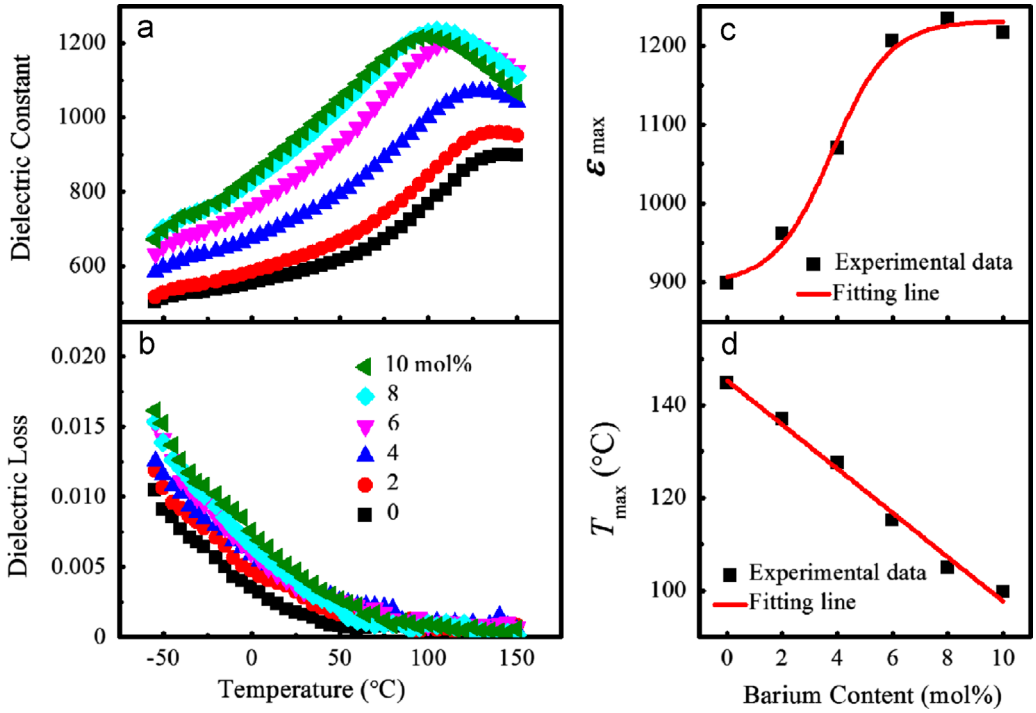

Fig. 4. (a) Dielectric constant and (b) dielectric loss spectra of the barium doped PLZST ceramics measured at 1 kHz. Dependences of (c) maximum dielectric constants ε_{max} and (d) the temperatures of phase transition from AFE to paraelectric T_{max} on the barium content.

The inset in Fig. 3 shows the enlarged region for the diffraction peaks at $2\theta=45^{\circ}$. A tetragonal antiferroelectric phase is detected in the range of $x \leq 0.08$, due to the splitting of the (200) peak. The splitting becomes more and more obvious with the increase of barium content. It has been well known that ferroelectric (FE) phase is stabilized for $\tau > 1$ and antiferroelectric (AFE) phase is stabilized for $\tau < 1$ [7]. As the barium content increases, the tolerance factor τ of the PLBZST ceramic derived from the substitution of Ba^{2+} for Pb^{2+} increases from 0.965 to 0.970, indicating the decreasing stability of the AFE phase and the increasing tetragonality of the unit cell.

The temperature dependence of the dielectric constant and loss for the PLBZST ceramics is given in Fig. 4(a) and (b), respectively. For all the compositions, the temperature at the maximum dielectric constants (T_{max}) was considered to be the temperature of the phase transition from AFE to parelectric phase. When the amount of barium content was increased from 0 to 10 mol%, the maximum dielectric constants ε_{max} increased from 900 to 1200 (Fig. 4(c)), and T_{max} decreased approximately by 4.8 °C/mol% (Fig. 4(d)), which may be related to the increase of tetragonality in the PLBZST ceramics by the substitution of Ba^{2+} ions with Pb^{2+} ions. The increased tetragonality of the unit cell and higher polarizability of Ba^{2+} enhance the ferroelectricity, leading to the increase of the dielectric constant and the reduction of T_{max}.

The *P–E* hysteresis loops of the PLBZST samples measured at room temperature are shown in Fig. 5(a). All the samples exhibited strongly slanted hysteresis loops. The switching field decreases with increasing barium content, which is due to the increase in the tetragonality of unit cell and the decrease in the stability of antiferroelectric phase. The charged energy storage density (J_c) is equal to integral of the area enclosed by charge curve and *y*-axis. The discharged energy storage density (J_d) is equal to integral of the area enclosed by discharge curve and *y*-axis. The energy storage efficiency η is equal to the ratio of J_d and J_c [20]. As shown in Fig. 5(b), both charged and discharged energy storage density increase sharply at first, and then decrease slightly with increasing barium content. The maximum energy storage density of 0.7 J/cm^3 is obtained at $x=0.06$. All the samples exhibit high energy storage efficiency, which is attributed to the slanted hysteresis loops of samples.

The discharge curves measured at 8 kV/mm for the PLBZST samples with various barium contents are shown in Fig. 6. According to the discharge curves, the discharge time increased with increasing barium content due to the increase in capacitance. Although the discharge curve varies greatly with variation of *RC*, the released energy density is nearly constant. Furthermore, the released energy density J_{d*} could be obtained by the following formula [21]:

$$J_{d*} = \frac{R}{V}\int I^2(t)dt \tag{4}$$

where $I(t)$ is the discharged current, t is the discharging time, R is the resistance of load (equal to R_4 in Fig. 1), and V is the volume of capacitor. The time dependence of the released energy densities J_{d*} of the PLBZST ceramics with various barium contents is illustrated in Fig. 7. The released energy densities increase at first and then decrease with increasing barium content, which corresponds to the behavior of the discharge energy storage density obtained from the hysteresis loops at the same amplitude of the electric field.

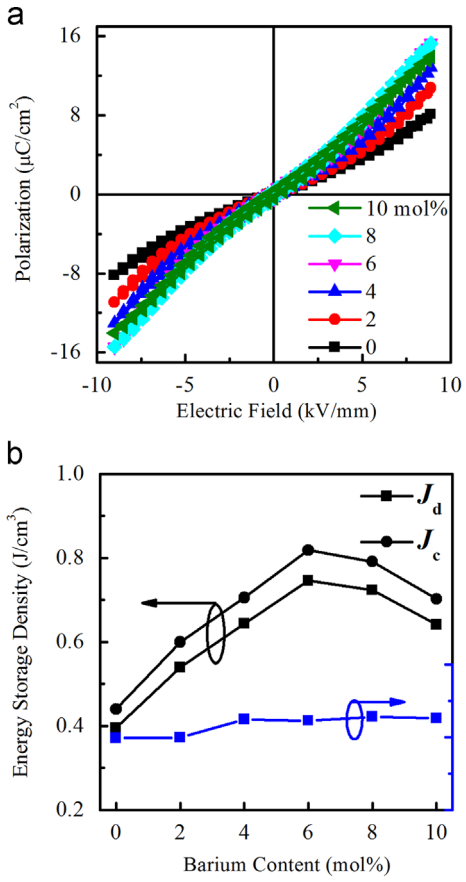

Fig. 5. (a) *P–E* loops of all samples at room temperature. (b) Charged energy storage density J_c, discharged energy storage density J_d and energy storage efficiency η of the barium doped PLZST ceramics as a function of the barium content.

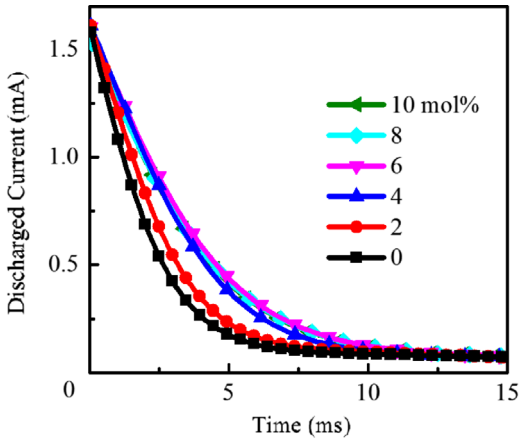

Fig. 6. The discharge curves for the barium doped PLZST ceramics after charging at 8 kV/mm.

The time dependence of the released energy densities J_{d*} after 1, 1000, 5000, and 10,000 charge–discharge cycles at 6.2 kV/mm is shown in Fig. 8(a) and (b), for undoped and 6 mol% barium doped PLZST ceramics, respectively. The released energy density decreases gradually with the increase of cycle numbers in both undoped and doped PLZST ceramics. The released energy density of the undoped PLZST ceramic

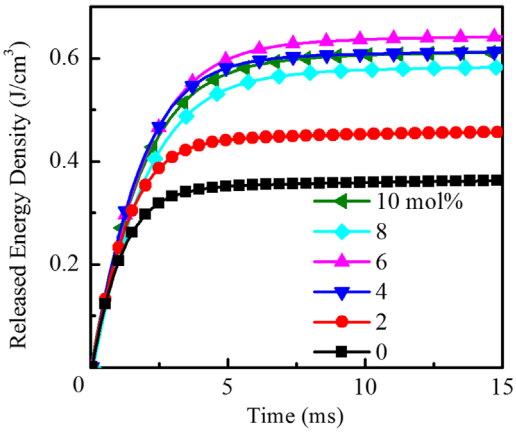

Fig. 7. Time dependence of the calculated released energy densities of the PLZST ceramics with various barium contents.

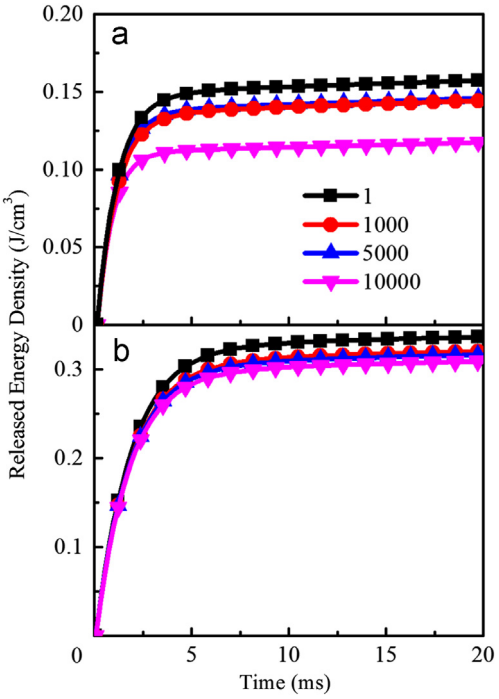

Fig. 8. The calculated released energy densities of (a) undoped and (b) 6 mol% barium doped PLZST ceramics after 1, 1000, 5000, and 10,000 charge–discharge cycles.

was reduced by 25% after 10,000 cycles, while only 8% energy density loss was observed for the 6 mol% barium doped PLZST ceramic. The better fatigue endurance of the barium doped PLZST ceramic is favorable to extend the charge–discharge cycling lifetime of pulsed power capacitors.

4. Conclusion

The barium doped PLZST ceramics were prepared by the solid state reaction, and their dielectric properties and energy storage performances were investigated. The diffraction peaks corresponding to the pyrochlore phase were gradually weakened with increasing x, and disappeared above $x=0.08$. In

addition, the increase of the barium content led to the increase of the maximum dielectric constant and the decrease of the transition temperature and the switching field. As a result, both charged and discharged energy storage density calculated from hysteresis loops and released energy densities obtained from discharge curves increased at first, and then decreased slightly with increasing barium content with the optimum value of the barium content at about 6 mol%. Moreover, the barium doped PLZST ceramics exhibited better fatigue endurance during charge–discharge cycling.

Acknowledgments

This work was supported by International Science & Technology Cooperation Program of China (No. 2012DFR50560) and National Natural Science Foundation of China (No. 51372014).

References

[1] X.H. Hao, Y. Wang, L. Zhang, L.W. Zhang, S.L. An, Composition-dependent dielectric and energy-storage properties of (Pb,La)(Zr,Sn,Ti)O_3 antiferroelectric thick films, Appl. Phys. Lett. 102 (2013) 163903.

[2] J.F. Wang, T.Q. Yang, S.C. Chen, G. Li, High energy storage density performance of Ba, Sr-modified lead lanthanum zirconate titanate stannate antiferroelectric ceramics, Mater. Res. Bull. 48 (2013) 3847–3849.

[3] Q.F. Zhang, T.Q. Yang, Y.Y. Zhang, J.F. Wang, X. Yao, Enhanced antiferroelectric stability and electric-field-induced strain properties in rare earth-modified Pb ($Zr_{0.63}$ $Sn_{0.26}$ $Ti_{0.11}$) O_3 ceramics, Appl. Phys. Lett. 102 (2013) 222904.

[4] X.H. Hao, J.W. Zhai, L.B. Kong, Z.K. Xu, A comprehensive review on the progress of lead zirconate-based antiferroelectric materials, Prog. Mater. Sci. 63 (2014) 1–57.

[5] N. Zhang, Y.J. Feng, Z. Xu, Effects of barium modification on dielectric and ferroelectric properties of PLZST ceramics, Mater. Res. Innov. 15 (2011) 240–243.

[6] J. Wang, T. Yang, S. Chen, G. Li, X. Yao, Characteristics and dielectric properties of ($Pb_{0.97-x}La_{0.02}Ba_x$)($Zr_{0.72}Sn_{0.22}Ti_{0.06}$)$O_3$ ceramics, J. Alloys Compd. 539 (2012) 280–283.

[7] S.E. Park, K. Markowski, S. Yoshikawa, L.E. Cross, Effect on electrical properties of barium and strontium additions in the lead lanthanum zirconate stannate titanate system, J. Am. Ceram. Soc. 80 (1997) 407–412.

[8] Y. Wang, K.F. Wang, C. Zhu, T. Wei, J.S. Zhu, J.M. Liu, Fatigue suppression of ferroelectric $Pb_{1-x}Ba_x(Zr_{0.52}Ti_{0.48})O_3$ thin films prepared by sol–gel method, J. Appl. Phys. 101 (2007) 046104.

[9] Y.H. Xu, H.Z. Guo, X.M. Liu, Y.J. Feng, X.L. Tan, Effect of Ba content on the stress sensitivity of the antiferroelectric to ferroelectric phase transition in (Pb,La,Ba,)(Zr,Sn,Ti)O_3 ceramics, J. Am. Ceram. Soc. 97 (2014) 206–212.

[10] B.Y. Ahn, N.K. Kim, Effects of barium substitution on perovskite formation, dielectric properties, and diffuseness characteristics of lead zinc niobate ceramics, J. Am. Ceram. Soc. 83 (2000) 1720–1726.

[11] H.L. Zhang, X.F. Chen, F. Cao, G.S. Wang, X.L. Dong, Z.Y. Hu, T. Du, Charge–discharge properties of an antiferroelectric ceramics capacitor under different electric fields, J. Am. Ceram. Soc. 93 (2010) 4015–4017.

[12] P. Wawrzała, J. Korzekwa, Charge–discharge properties of PLZT x/90/10 ceramics, Ferroelectrics 446 (2013) 91–101.

[13] M.T. Domonkos, S. Heidger, D. Brown, J.V. Parker, C.W. Gregg, K. Slenes, W. Hackenberger, S. Kwon, E. Loree, T. Tran, Submicrosecond pulsed power capacitors based on novel ceramic technologies, IEEE Trans. Plasma Sci. 38 (2010) 2686–2693.

[14] B.M. Xu, P. Moses, N.G. Pai, L.E. Cross, Charge release of lanthanum-doped lead zirconate titanate stannate antiferroelectric thin films, Appl. Phys. Lett. 72 (1998) 593–595.

[15] B.J. Chu, X. Zhou, K.L. Ren, B. Neese, M.R. Lin, Q. Wang, F. Bauer, Q.M. Zhang, A dielectric polymer with high electric energy density and fast discharge speed, Science 313 (2006) 334–336.

[16] H. Tang, H.A. Sodano, Ultra high energy density nanocomposite capacitors with fast discharge using $Ba_{0.2}Sr_{0.8}TiO_3$ nanowires, Nano Lett. 13 (2013) 1373–1379.

[17] S. Švarcová, K. Wiik, J. Tolchard, H.J. Bouwmeester, T. Grande, Structural instability of cubic perovskite $Ba_xSr_{1-x}Co_{1-y}Fe_yO_{3-\delta}$, Solid State Ionics 178 (2008) 1787–1791.

[18] I.M. Reaney, E.L. Colla, N. Setter, Dielectric and structural characteristics of Ba-and Sr-based complex perovskites as a function of tolerance factor, Jpn. J. Appl. Phys. 33 (1994) 3984–3990.

[19] R. Shannon, Revised effective ionic radii and systematic studies of interatomic distances in halides and chalcogenides, Acta Crystallogr. Sect. A 32 (1976) 751–767.

[20] Y. Zhang, J.J. Huang, T. Ma, X.R. Wang, C. Deng, X.M. Dai, Sintering temperature dependence of energy-storage properties in (Ba,Sr)TiO_3 glass–ceramics, J. Am. Ceram. Soc. 94 (2011) 1805–1810.

[21] X. Hao, A review on the dielectric materials for high energy-storage application, J. Adv. Dielectr. 3 (2013) 1330001.